# Gold Nanocages: Engineering Their Structure for Biomedical Applications**

By *Jingyi Chen*, *Benjamin Wiley*, *Zhi-Yuan Li*, *Dean Campbell*, *Fusayo Saeki*, *Hu Cang*, *Leslie Au*, *Jennifer Lee*, *Xingde Li*, and *Younan Xia**

The galvanic replacement reaction between a Ag template and $HAuCl_4$ in an aqueous solution transforms 30–200 nm Ag nanocubes into Au nanoboxes and nanocages (nanoboxes with porous walls). By controlling the molar ratio of Ag to $HAuCl_4$, the extinction peak of resultant structures can be continuously tuned from the blue (400 nm) to the near-infrared (1200 nm) region of the electromagnetic spectrum. These hollow Au nanostructures are characterized by extraordinarily large cross-sections for both absorption and scattering. Optical coherence tomography measurements indicate that the 36 nm nanocage has a scattering cross-section of $\sim 0.8 \times 10^{-15}$ m$^2$ and an absorption cross-section of $\sim 7.3 \times 10^{-15}$ m$^2$. The absorption cross-section is more than five orders of magnitude larger than those of conventional organic dyes. Exposure of Au nanocages to a camera flash resulted in the melting and conversion of Au nanocages into spherical particles due to photothermal heating. Discrete-dipole-approximation calculations suggest that the magnitudes of both scattering and absorption cross-sections of Au nanocages can be tailored by controlling their dimensions, as well as the thickness and porosity of their walls. This novel class of hollow nanostructures is expected to find use as both a contrast agent for optical imaging in early stage tumor detection and as a therapeutic agent for photothermal cancer treatment.

## 1. Introduction

Since Faraday first prepared Au colloids by reducing an aqueous solution of gold chloride with phosphorus in 1856, the interaction between light and Au nanoparticles has fascinated the scientific community.[1] The ruby-red color of Faraday's Au colloidal suspensions is due to their strong interaction with visible light at around 520 nm. At this wavelength, free electrons in the Au nanoparticles collectively oscillate and scatter/absorb the incident electromagnetic wave, a phenomenon known as surface plasmon resonance (SPR).[2] In 1908, Mie presented a formula for calculating the wavelength-dependent scattering and absorption cross-sections of a solid spherical particle composed of a material with a known refractive index, and with dimensions less than the wavelength of light.[3] Although Mie developed his theory to determine the size of Au particles, the theory has proved extremely useful for predicting and explaining the extinction (extinction = scattering + absorption) spectra of colloidal particles made of various materials, and has only recently been supplanted by other computational methods.

Spherical Au particles 40 nm in diameter have extinction peaks centered at 520 nm. The peaks of smaller particles (1–20 nm in diameter) are slightly blue-shifted to 510 nm, while those of larger particles (140 nm in diameter) are red-shifted to 650 nm. The location of SPR peaks in the visible region is instrumental to various colorimetric applications that involve the use of the naked eye to detect color changes.[4] However, for biomedical applications that require deeper penetration of near-infrared light (800–1200 nm), to which both blood and soft tissues are highly "transparent", a differ-

[*] Prof. Y. Xia, J. Chen, Prof. D. Campbell, Dr. H. Cang, L. Au, J. Lee
Department of Chemistry, University of Washington
Seattle, WA 98195 (USA)
E-mail: xia@chem.washington.edu
B. Wiley
Department of Chemical Engineering, University of Washington
Seattle, WA 98195 (USA)
Prof. Z.-Y. Li
Institute of Physics, Chinese Academy of Sciences
Beijing 10080 (P.R. China)
Dr. F. Saeki, Prof. X. Li
Department of Bioengineering, University of Washington
Seattle, WA 98195 (USA)

[**] This work has been supported in part by a DARPA-DURINT subcontract from Harvard University and a fellowship from the David and Lucile Packard Foundation. Y. X. is an Alfred P. Sloan Research Fellow and a Camille Dreyfus Teacher Scholar. J. C. and B. W. thank the Center for Nanotechnology at the UW for a Nanotech Student Fellowship Award and an IGERT Fellowship Award (supported by the NSF, DGE-9987620), respectively. Z.-Y. L. is supported by the National Key Basis Research Special Foundation of China (No. 2004 CB719804). X. L. acknowledges the support from the National Science Foundation (Career Award) and F. S. acknowledges a fellowship from the NIH GI Training grant. Part of the work was performed at the Nanotech User Facility (NTUF), a member of the National Nanotechnology Infrastructure Network (NNIN) funded by the NSF. D. C. is on sabbatical leave from the Bradley University.

 DOI: 10.1002/adma.200500833  

ent type of Au nanostructure is required. At least three different approaches have been demonstrated to shift the SPR peaks of Au nanoparticles to the near-infrared region: i) by forming aggregates from spherical Au nanoparticles;[5] ii) by elongating spherical nanoparticles into Au nanorods;[6] and iii) by emptying the interiors of spherical nanoparticles to form hollow Au nanostructures.[7] The last approach is particularly interesting and attractive. As calculated by Neeves and Birnboim in 1989, a composite spherical particle consisting of a metallic shell and a dielectric core could give rise to SPR modes with their wavelengths variable over a broad range of the electromagnetic spectrum.[8]

Although the SPR properties of hollow Au nanostructures have been studied for many years as a theoretical model, it has been a challenge to verify the predictions experimentally. Halas and co-workers were the first to produce Au shells with an SPR peak in the near-infrared by coating silica or polymer beads with Au shells of variable thickness.[9] More recently, we demonstrated that Ag nanostructures could serve as a template for galvanic replacement with $HAuCl_4$ to make complementary hollow Au nanostructures with controllable void size, wall thickness, and wall porosity.[10] For example, with Ag nanocubes as a template, Au nanoboxes (with non-porous walls) or nanocages (with porous walls) could be routinely produced on relatively large scales. Because the dimension and wall thickness of the resultant Au nanocages are well controlled by the molar ratio of Ag to $HAuCl_4$, their SPR peaks can be conveniently and precisely shifted to cover a spectral region from 400 to 1200 nm.

In general, hollow and porous Au nanostructures can be synthesized from Ag nanoparticles of any morphology (e.g., multiply twinned quasispheres that can be prepared on the industrial scale using a number of methods). We have largely focused on nanocubes because they can be readily prepared as monodisperse samples with their sizes controllable from 30 to 200 nm. Because Ag nanocubes are single crystals, the Au nanocages derived from them are essentially single crystalline too, and therefore exhibit much stronger mechanical strength than polycrystalline samples. That is probably why the Au nanocages derived from Ag nanocubes can survive the strong capillary forces involved in solvent evaporation (during sample drying) even though their walls are porous and usually 2–3 nm thick. Here we present some recent developments related to the synthesis, optical characterization, and niche applications of Au nanocages.

## 2. Polyol Synthesis of Ag Nanocubes

We have demonstrated a chemical approach to the facile synthesis of Ag nanostructures as uniform samples, in relatively large quantities, and with a variety of well-controlled shapes that include cubes, tetrahedrons, quasispheres, rods, and wires.[11] The synthesis is built upon the polyol process,[12] in which a polyol (e.g., ethylene glycol) serves as both solvent and reducing agent. In a typical synthesis, $AgNO_3$ is added to and reduced by ethylene glycol at an elevated temperature to generate Ag nanocrystals (or seeds). More Ag atoms are then added to these seeds as $AgNO_3$ is continuously reduced. In the presence of poly(vinylpyrrolidone) (PVP)—a polymer capable of selectively binding to the (100) surface [13]—the addition of Ag atoms to the surfaces of seeds can be directed to generate Ag nanostructures with well-defined and controllable shapes. For example, because PVP passivates the {100} sides of rods, atoms preferentially add to the {111} facets on the ends. This mechanism produces Ag nanowires tens of micrometers in length and with diameters around 50 nm.

A similar mechanism is also responsible for the growth of nanocubes, where preferential addition of Ag atoms to the {111} facets of a single-crystal seed leads to the formation of sharp corners. The as-synthesized Ag nanostructures are covered by PVP; they can be harvested from the reaction solution through centrifugation, and re-dispersed into other solvents such as water for subsequent applications. Since each product only contains nanoparticles of a specific shape, no additional separation or purification is needed. The key to high yields of nanocubes is to control the seed crystallinity. In the presence of chloride, twinned seeds could be selectively etched by the oxygen in air to leave only single-crystal seeds in the reaction solution.[14] Single-crystal seeds subsequently grow to generate Ag nanocubes of 30 to 200 nm in edge length, with size controlled by reaction time. Figure 1 shows scanning electron microscopy (SEM) images of four typical examples with sizes ranging from 30 to 200 nm, and with various degrees of corner truncation. All these samples are single crystals, as confirmed by their electron-diffraction patterns.

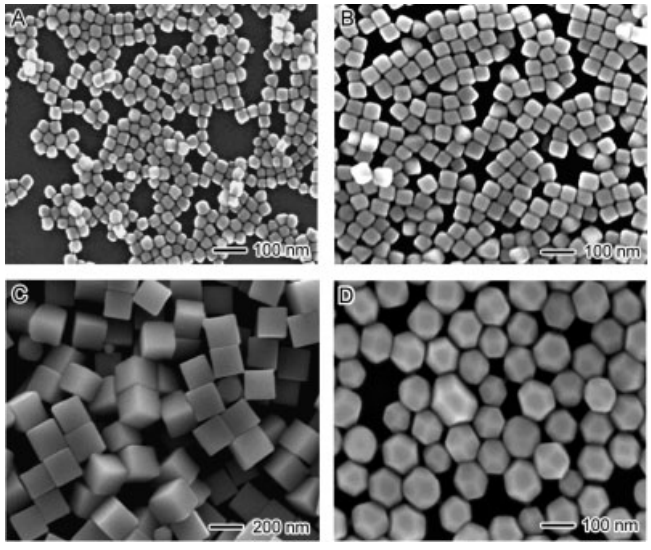


**Figure 1.** SEM images of four typical examples of Ag nanocubes: A–C) cubes 30, 50, and 200 nm in edge length and D) truncated cubes 100 nm in diameter.

  

ADVANCED MATERIALS



## 3. Transformation of Ag Nanocubes into Au Nanocages

Because Ag is more reactive than Au, $HAuCl_4$ can be reduced by Ag nanostructures to generate Au atoms:

$$3Ag(s) + AuCl_4^-(aq) \rightarrow Au(s) + 3Ag^+(aq) + 4Cl^-(aq) \quad (1)$$

During this replacement reaction, Au atoms epitaxially nucleate, grow into small islands, and eventually evolve into a thin shell around each Ag template. The product is a hollow structure with an inner void complementary to that of the Ag template. Based on the stoichiometry (and confirmed by transmission electron microscopy (TEM) studies), the wall thickness is approximately one-eighteenth of the dimension of the Ag template. By performing the reaction in aqueous medium under reflux, the $Ag^+$ and $Cl^-$ species can be kept in the ionic state without forming AgCl precipitate, which may otherwise interfere with the galvanic replacement reaction.

We have systematically investigated the mechanism involved in the galvanic replacement reaction between Ag nanocubes 110 nm in edge length and $HAuCl_4$.[15] The results from this system indicate that the replacement proceeds through three major steps: i) initiation of galvanic replacement by pitting at a specific site on the surface of a Ag nanocube; ii) the formation of a pinhole-free nanobox consisting of thin, uniform walls (made of a Au/Ag alloy) through a combination of galvanic replacement (between Ag and $AuCl_4^-$) and alloying (between Ag and Au); and iii) the generation of pores in the wall through a dealloying process, in which Ag atoms are selectively oxidized. As galvanic replacement, alloying, and dealloying proceed, the Ag nanocube template is gradually dissolved, leading first to the formation of a Au nanobox, and then to a series of nanocages with increasing porosities. The dimensions, wall thickness, pore sizes, and pore densities of the resultant Au nanocages can all be controlled by varying the molar ratio between Ag nanocubes and $HAuCl_4$ in a fashion similar to acid–base titration.

As shown in Figure 2A, the same mechanism is still applicable to Ag nanocubes as small as 30 nm in edge length. These TEM images correspond to the representative structures observed at different stages of the reaction. Similar to large nanocubes, the reaction is initiated on one of the six {100} faces of a cube, probably from a defect site that has the highest free energy. As Ag is dissolved from this site, Au atoms are formed and deposited around the Ag nanocube. Since the lattice constants of Ag and Au are essentially the same, Ag atoms can diffuse from the cube into the Au shell to form an alloy. At a specific molar ratio between Ag and $HAuCl_4$, a completely closed nanobox consisting of a Au/Ag alloy is formed. If more $HAuCl_4$ is added, dealloying causes small holes to appear on the {111} corner facets (see Fig. 2B for an SEM image). In the late stage of dealloying, small holes can also be formed on the {100} facets. Eventually, the nanocage breaks up into small pieces (not shown in Fig. 2A) when the porosity becomes too high to support the structure. There are two major differences between 30 nm and 110 nm Ag nanocubes: i) in the early stage of dealloying, the 30 nm cubes do not go through structural reconstruction to form nanoboxes with significantly truncated corners; and ii) smaller Ag cubes tend to yield Au nanocages with a higher surface coverage of holes than the larger ones.

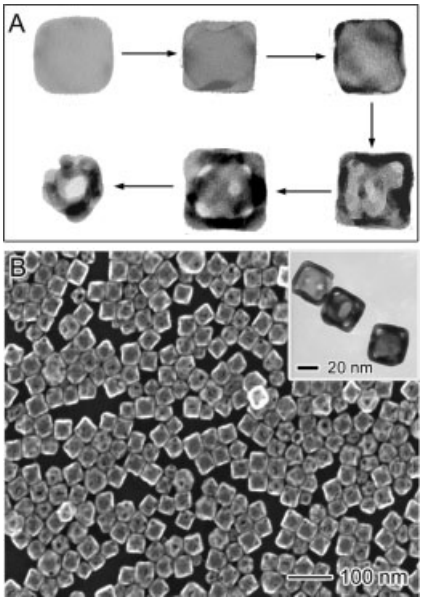


**Figure 2.** A) TEM images detailing all morphological and structural changes involved in the galvanic replacement reaction between Ag nanocubes 30 nm in edge length and $HAuCl_4$. B) A typical SEM image of Au nanocages derived from Ag nanocubes of 30 nm in edge length. The inset shows the corresponding TEM image.

## 4. Optical Characterization of Au Nanocages

As the nanostructures change from solid cubes to hollow boxes and porous cages, their SPR peak is continuously shifted toward longer wavelengths. Figure 3 shows the UV-

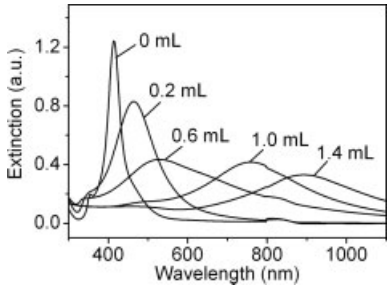


**Figure 3.** UV-vis-NIR extinction spectra taken from an aqueous solution of Ag nanocubes (30 nm in edge length) after it has been titrated with different volumes of a 0.2 mM $HAuCl_4$ solution (as labeled on each curve). The titration was performed by adding different volumes of $HAuCl_4$ to 5 mL aqueous solution containing 75 μL of the as-synthesized Ag nanocubes and 1 μM PVP (molecular weight $MW = 55\,000$ g mol$^{-1}$). Note that the SPR peak continuously red-shifted toward the near-IR region as the volume of $HAuCl_4$ was increased.

  

vis-near IR (NIR) extinction spectra obtained from titrating an aqueous solution of 30 nm Ag nanocubes with different volumes of $HAuCl_4$. Although the volume of these cubes was 1/50 of the 110 nm cubes previously studied, the SPR peak of resultant Au nanocages could still be tuned to the near-infrared region before the cages broke up into small particles. Our discrete-dipole-approximation (DDA) calculations (see Sec. 5) suggest that peak broadening is likely due to small variations in the wall thickness. For example, even a 2 nm difference in the wall thickness can cause a 110 nm peak shift. The variation in wall thickness may also contribute to the decrease in SPR peak intensity. The calculations shown in Section 5 suggest that the decrease in SPR peak intensity could be attributed to the increase in wall porosity. As more $HAuCl_4$ solution was introduced, the total concentration of all nanocages with different wall thicknesses was also gradually reduced.

The concentration of each batch of Au nanocages can be determined from the intensity of the SPR peak using the Beer–Lambert law. Figure 4A shows the extinction spectra taken from an aqueous dispersion of Au nanocages (derived from 30 nm Ag cubes) as it was continuously diluted with water. The intensity of the SPR peak linearly decreased with decreasing concentrations of Au nanocages. Figure 4B plots the peak extinction at 787 nm against the concentration of Au nanocages, which was assumed to be equal to the concentration of Ag nanocubes measured using atomic emission spectroscopy. The relationship between the intensity of the SPR peak and the concentration follows the Beer–Lambert law, from which the extinction cross-section was estimated to be $\sim 1.3 \times 10^{-15}$ m$^2$. The nonlinearity at high concentrations is probably caused by multiple scattering effects.

The large absorption cross-section of Au nanocages implies that they might be an ideal contrast agent for optical imaging, namely, optical coherence tomography (OCT).[16] To demonstrate this potential, OCT imaging was performed on phantom samples with and without Au nanocages (derived from 30 nm Ag cubes and with the SPR peak tuned to ~800 nm). The phantom was made of gelatin embedded with $TiO_2$ granules to mimic the scattering background of typical biological tissues. OCT imaging was conducted using a 7 fs Ti:sapphire laser with a center wavelength at 825 nm. As the laser was scanned over the tissue phantom, the intensity of back-scattered light was measured as a function of depth. By fitting the decay curve (OCT signal intensity vs. sample depth) to an analytical expression that describes the OCT axial scan and subtracting out the scattering of $TiO_2$, we estimated that the scattering cross-section ($C_{sca}$) and absorption cross-section ($C_{abs}$) of the Au nanocages were $\sim 0.8 \times 10^{-15}$ and $\sim 7.3 \times 10^{-15}$ m$^2$, respectively. The ratio of the absorption to scattering cross-section was 9. Note that the extinction cross-section ($\sim 8.1 \times 10^{-15}$ m$^2$) obtained from OCT measurements and the one estimated from the Beer–Lambert law are within the same order of magnitude. The measured absorption cross-section of Au nanocages is at least five orders larger than previously used organic dyes, suggesting that Au nanocages represent a new class of absorption-contrast agents for OCT imaging.

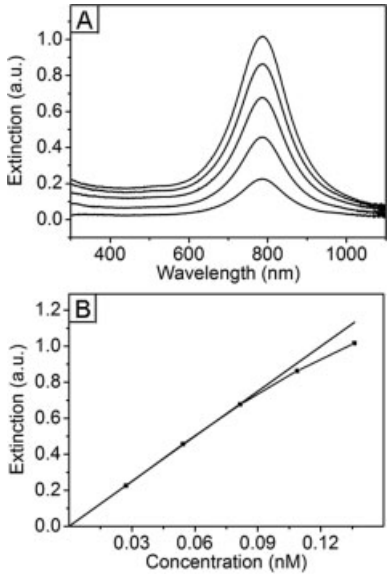


**Figure 4.** A) Extinction spectra of the Au nanocages shown in Figure 2B, which were prepared as dispersions of different concentrations. B) A plot showing the dependence of peak extinction on the concentration of Au nanocages. Note that the data points (■) deviate from the linear fitting when the concentration was higher than 0.09 nM.

## 5. Calculation of the Scattering and Absorption Properties of Au Nanocages

Both the scattering and absorption coefficients of a spherical nanoparticle can be computed using the Mie theory, as long as the dispersion curve of the material is known.[3] However, Mie's formula can only be applied to systems with spherical symmetry. In the past decade, a number of numerical methods have been developed to calculate the scattering and absorption coefficients of nanoparticles with arbitrary shapes. Examples include the DDA, T-matrix, and spectral representation methods.[17] DDA is a computational method capable of studying both scattering and absorption of electromagnetic radiation by particles with sizes on the order of, or less than, the wavelength of the incident light. In the DDA method, the particle is approximated by a sufficiently large array of polarizable point dipoles.[18] The scattering and absorption cross-sections of the particle can be obtained once the location and polarizability of each individual unit have been specified.

We have applied the DDA method to investigate the scattering and absorption properties of Au nanoboxes and nanocages. Figures 5A,B compare the calculated extinction cross-section ($C_{ext}$), $C_{abs}$, and $C_{sca}$ (note that $C_{ext} = C_{abs} + C_{sca}$) for Au nanoboxes 60 and 40 nm in edge length, respectively, with a wall thickness of 5 nm for each. The refractive index of bulk

  

ADVANCED MATERIALS



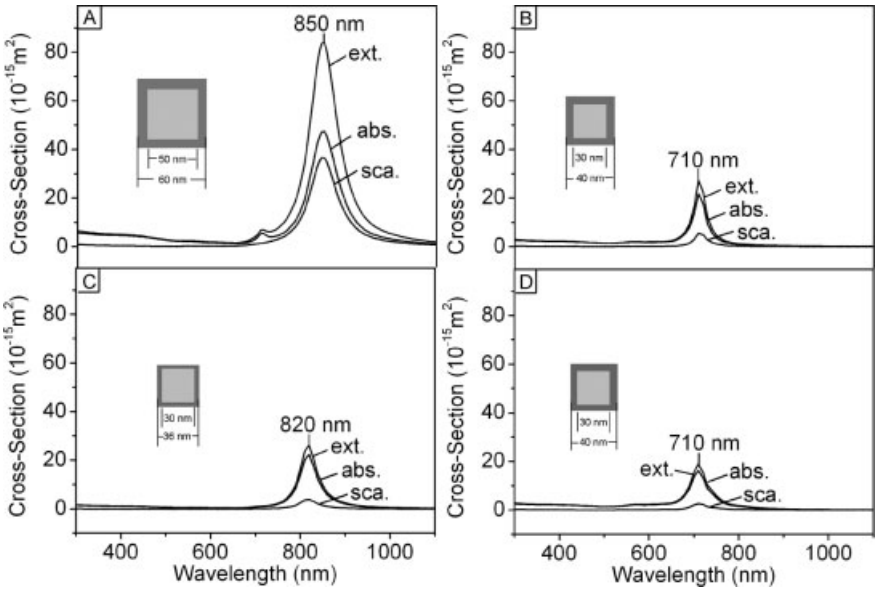


**Figure 5.** Extinction spectra calculated using the DDA method for Au nanocages having four different sets of geometric parameters: A) a Au nanobox 50 nm in inner edge length and 5 nm in wall thickness; B) a Au nanobox 30 nm in inner edge length and 5 nm in wall thickness; C) the same as in (B), except that the wall thickness is 3 nm; and D) the same as in (B), except that the eight corners are decorated with triangular holes 5 nm in edge length.

gold was used, and the nanobox was assumed to be surrounded by and completely filled with water. Compared with organic chromophores, the calculated absorption cross-section of Au nanocages is at least five orders of magnitude larger. Similar to solid Au nanoparticles, light absorption dominates the extinction spectra for Au nanoboxes of relatively small sizes (< 30 nm), and light scattering increases for nanoboxes of larger dimensions (> 60 nm).

Figure 5C shows the cross-sections calculated for a Au nanobox whose edge length and wall thickness are 36 and 3 nm, respectively. Compared with Figure 5B, the extinction peak is red-shifted from 710 to 820 nm as the wall thickness is reduced from 5 to 3 nm. However, the magnitudes of both scattering and absorption cross-sections have only a slight dependence on the wall thickness. Figure 5D shows the calculated spectra of a Au nanobox similar to that used for Figure 5B, except that all eight corners were replaced with holes to form a nanocage. It is obvious that an increase in porosity of the nanocage caused a significant reduction in the magnitude of scattering and absorption cross-sections. In fact, our calculations indicate that the scattering and absorption cross-sections of a 40 nm Au nanocage linearly decrease from $5.5\times10^{-15}$ to $2.6\times10^{-15}$ and $21.7\times10^{-15}$ to $16.2\times10^{-15}$ m$^2$, respectively, when the number of corners with holes is increased from 0 to 8. In contrast to wall thickness, the position of the extinction peak does not show any significant dependence on the porosity of the nanobox.

The peak positions of the extinction curves calculated using the DDA method match well with the experimentally measured bulk spectra. The minor discrepancy in the peak width can be attributed to the fact that the nanocages in a real sample might have a distribution in size and wall thickness, as well as different degrees of corner truncation. In addition to fine-tuning of the extinction-peak position, we can tailor the magnitudes of both scattering and absorption cross-sections by controlling the size and porosity of Au nanocages, and thereby enhance their versatility for biomedical applications.

## 6. Photothermal Effect of Au Nanocages

The extremely large absorption cross-section of Au nanocages suggests their potential use as a photothermal therapeutic agent. Under exposure to near-infrared light, nanocages selectively attached to cancer cells could induce localized heating to kill those cancer cells. Unlike current chemotherapies, it has been demonstrated that Au nanoshells and near-infrared light by themselves do not harm healthy tissue.[19]

As an initial demonstration of this photothermal effect, we exposed Au nanocages supported on a copper TEM grid (coated with carbon) to a camera flash (Vivitar 90, Japan).[20] Surprisingly, a brief flash of light increased the temperature of the nanocages past their melting point. Figure 6A shows a sample of Au nanocages before exposure to a camera flash. After 10 exposures, the Au nanocages were completely melted, and surface tension forced many of the Au droplets into nearly spherical shapes (Fig. 6B). The key to the success of this demonstration is that the heat resulting from the photothermal conversion could not easily dissipate through the surrounding materials (e.g., air and thin carbon film), which were in contact with the Au nanocages. Although the generation and transport of heat during the flash requires a more systematic study, this simple experiment serves to demonstrate the potential of the photothermal effect for future therapeutic applications of Au nanocages.

## 7. Bioconjugation of Au Nanocages for Targeting Cancer Cells

The Au nanocages can also be functionalized with biological molecules to target cancer cells for early-stage diagnosis and photothermal therapy of cancers.[16] For example, Au nanocages have been conjugated with an antibody following the two-step protocol shown in Figure 7A. In the first step, succinimidyl propionyl poly(ethylene glycol) disulfide (*N*-hy-

  

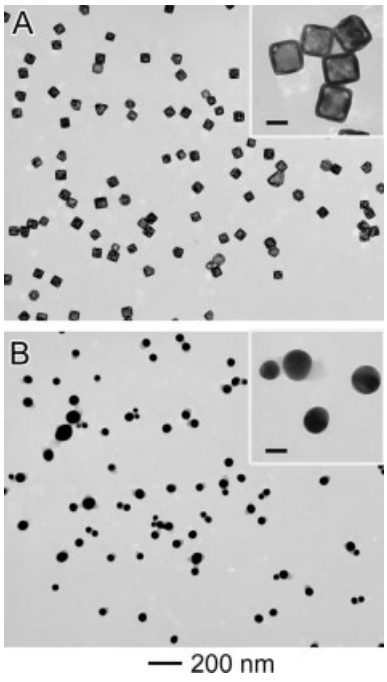


**Figure 6.** TEM images of Au nanocages (55 nm in edge length) A) before and B) after exposure to a camera-flash light. The insets are the enlarged TEM images, with the scale bars being 50 nm. Note that the nanocages melted and became spherical droplets due to the photothermal effect.

droxy succinimidyl (NHS)-activated poly(ethylene glycol), $MW = 1109\ \mathrm{g\,mol^{-1}}$) was bonded to the surface of an Au nanocage (Fig. 7A) by breaking its internal disulfide bond and forming a Au–S linkage. In the second step, the NHS-functionalized Au nanocage was reacted with the primary amine of an antibody. Both steps caused some minor shifts (< 10 nm) in the SPR peak associated with Au nanocages due to a refractive index change.

A breast-cancer cell line, SK-BR-3, which over expresses epidermal growth factor receptor 2 (EGFR2, or HER2),[21] was used to examine the molecular-specific binding of the bioconjugated Au nanocages. In a typical procedure, the primary antibody (monoclonal anti-HER2 antibody from a mouse) was first immobilized on the cancer cells by incubating the SK-BR-3 cells in a buffer containing anti-HER2 antibodies. A buffer solution containing immunoglobulin G-conjugated Au nanocages was then applied to the SK-BR-3 cells bound with anti-HER2 antibody, followed by extensive washing. Figure 7B shows the distribution of Au nanocages on the surface of an SK-BR-3 cell as revealed by SEM. Gold nanocages did not specifically attach to cells in control experiments where no anti-HER2 was applied. The results of these studies clearly establish that the bioconjugated Au nanocages can indeed serve as molecular probes to target a specific cancer cell line.

## 8. Concluding Remarks

Selective etching of twinned silver seeds during the reduction of $AgNO_3$ by ethylene glycol resulted in a nanocube

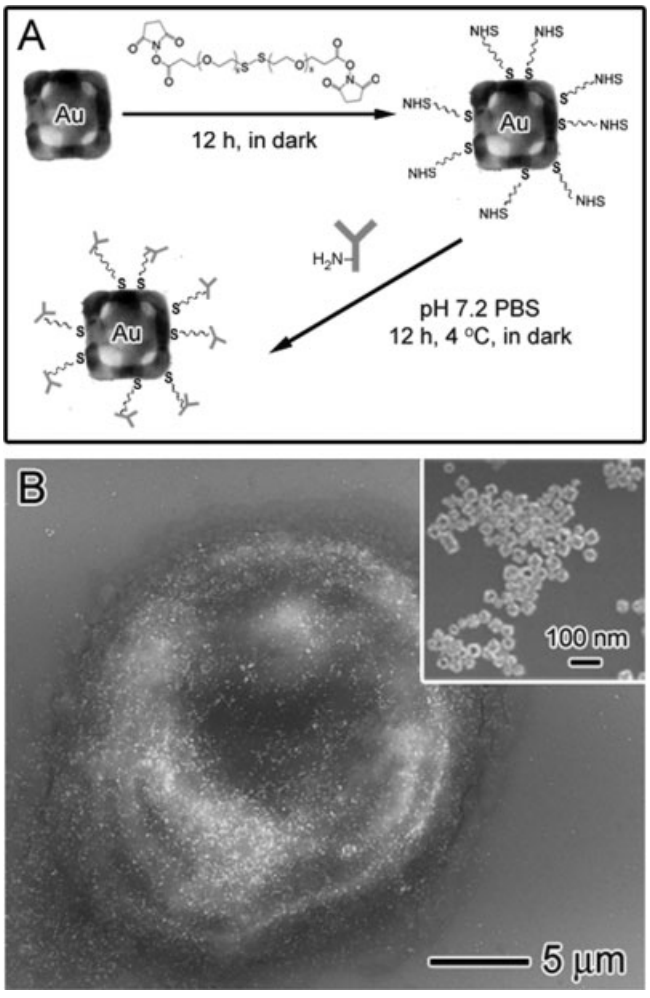


**Figure 7.** A) A schematic illustration of the two-step protocol used to conjugate antibodies to the surface of a gold nanocage. B) SEM image of an SK-BR-3 cancer cell whose surface was derivatized with primary anti-HER2 antibodies and then IgG-conjugated Au nanocages. The inset shows an SEM image at higher magnification, indicating that the Au nanocages were dispersed as a submonolayer on the cell surface.

product with well-controlled size, shape, and truncation. Because of their monodispersity, the nanocubes (30–200 nm in edge length) proved to be an ideal template for generating Au nanoboxes and nanocages through a galvanic replacement reaction between Ag and $HAuCl_4$. By simply controlling the molar ratio of Ag to $HAuCl_4$, we could tune the SPR peaks of the resultant nanostructures to any specific wavelength in the range 400 to 1200 nm. DDA calculations suggest that the observed red-shift of the SPR peak with increasing $HAuCl_4$ is mainly due to a reduction of wall thickness. Our preliminary results from both OCT imaging and photothermal-melting studies clearly establish that these Au nanocages strongly absorb and scatter light in the near-infrared region, with their absorption cross-sections at least five orders of magnitude larger than those of conventional organic dyes.

The remarkable SPR properties and biocompatibility of Au nanocages make them promising both as a contrast agent for

  

ADVANCED MATERIALS



in-vivo optical detection of cancers and as a therapeutic agent for photothermal treatment of cancers. Perhaps the two most significant thrusts in the fight against cancer are aimed at detection of cancers at early stages, which significantly improves survival rates, and at targeted cancer treatments that minimize damage to healthy tissue. By far the most prevalent method for cancer detection is biopsy, which is invasive and suffers a high sampling error. Progress has been made in the discovery and detection of biomarkers, which indicate the presence of cancers. However, only a few cancer biomarkers have been discovered, and the detection of miniscule amounts of a specific protein in a complex biological sample is still very challenging. New cancer treatments are under extensive investigation, but a general approach that has the power of chemotherapy without severe side effects is still lacking. We believe that functionalization of Au nanocages with cancer-specific antibodies may enable them to fulfill the critical needs of cancer detection and treatment simultaneously.

Although polystyrene or silica beads coated with Au shells have already been demonstrated for applications related to both cancer diagnosis and treatment,[19] the Au nanocages described above offer additional attractive features: i) the SPR peak of Au nanocages can be conveniently and precisely tuned to any wavelength in the spectral region from 400 to 1200 nm by simply controlling the molar ratio of Ag to $HAuCl_4$ in a fashion similar to acid–base titration; ii) both the scattering and absorption cross-sections of Au nanocages can be varied independently by changing the void size and the size or density of pores in the wall; iii) Au nanocages can be made extremely compact (< 30 nm) while still exhibiting a strong resonance peak that is tunable in the visible and near-infrared region; and iv) using the well-established alkanethiol chemistry, biofunctionalization of Au nanocages can be achieved in two steps that simply involve mixing and centrifugation.

Received: April 23, 2005
Published online: July 29, 2005

[1] M. Faraday, *Philos. Trans. R. Soc. London* **1857**, *147*, 145.
[2] U. Kreibig, M. Vollmer, *Optical Properties of Metal Clusters*, Springer, New York **1995**.
[3] G. Mie, *Ann. Phys.* **1908**, *25*, 337.
[4] R. Elghanian, J. J. Storhoff, R. C. Mucic, R. L. Letsinger, C. A. Mirkin, *Science* **1997**, *277*, 1078.
[5] a) C. G. Blatchford, J. R. Campbell, J. A. Creighton, *Surf. Sci.* **1992**, *120*, 435. b) M. Quinten, U. Kreibig, *Surf. Sci.* **1986**, *172*, 557.
[6] a) S. Link, M. El-Sayed, *J. Phys. Chem. B* **1999**, *103*, 8410. b) B. van der Zande, M. R. Bhmer, L. G. J. Fokkink, C. Schonenberger, *J. Phys. Chem. B* **1997**, *101*, 852. c) C. A. Foss, G. L. Hornyak, J. A. Stockert, C. R. Martin, *J. Phys. Chem.* **1994**, *98*, 2963. d) S. Chang, S. Chao-Wen, C. Chemg-Dah, L. Wei-Cheng, C. R. C. Wang, *Langmuir* **1999**, *15*, 701. e) C. J. Murphy, N. R. Jana, *Adv. Mater.* **2002**, *14*, 80. f) F. Kim, J. H. Song, P. Yang, *J. Am. Chem. Soc.* **2002**, *124*, 14 316.
[7] J. L. West, N. J. Halas, *Annu. Rev. Biomed. Eng.* **2003**, *5*, 285.
[8] a) A. E. Neeves, M. H. Birnboim, *J. Opt. Soc. Am. B* **1989**, *6*, 787. b) A. L. Aden, M. Kerker, *J. Appl. Phys.* **1951**, *22*, 1242.
[9] a) S. J. Oldenburg, R. D. Averitt, S. L. Westcott, N. J. Halas, *Chem. Phys. Lett.* **1998**, *288*, 243. b) F. Caruso, M. Spasova, V. Salgueirino-Maceira, L. M. Liz-Marzan, *Adv. Mater.* **2001**, *13*, 1090.
[10] a) Y. Sun, B. T. Mayers, Y. Xia, *Adv. Mater.* **2003**, *15*, 641. b) Y. Sun, Y. Xia, *Nano Lett.* **2003**, *3*, 1569. c) Y. Sun, B. T. Mayers, Y. Xia, *Nano Lett.* **2002**, *2*, 481.
[11] a) B. Wiley, Y. Sun, B. Mayers, Y. Xia, *Chem. Eur. J.* **2005**, *11*, 454. b) B. Wiley, Y. Sun, J. Chen, H. Cang, Z.-Y. Li, X. Li, Y. Xia, *MRS Bull.*, **2005**, *30*, 356.
[12] F. Fievet, J. P. Lagier, M. Figlarz, *MRS Bull.* **1989**, *14*, 29.
[13] a) Y. Sun, Y. Xia, *Science* **2002**, *298*, 2176. b) Y. Sun, B. Mayers, T. Herricks, Y. Xia, *Nano Lett.* **2003**, *3*, 955. c) Y. Sun, B. Gates, B. Mayers, Y. Xia, *Nano Lett.* **2002**, *2*, 165.
[14] a) B. Wiley, T. Herricks, Y. Sun, Y. Xia, *Nano Lett.* **2004**, *4*, 1733. b) S. H. Im, Y. T. Lee, B. Wiley, Y. Xia, *Angew. Chem. Int. Ed.* **2005**, *44*, 2154.
[15] Y. Sun, Y. Xia, *J. Am. Chem. Soc.* **2004**, *126*, 3892.
[16] J. Chen, F. Saeki, B. Wiley, H. Cang, M. J. Cobb, Z.-Y. Li, L. Au, H. Zhang, M. B. Kimmey, X. Li, Y. Xia, *Nano Lett.* **2005**, *5*, 473.
[17] *Light Scattering by Nonspherical Particles* (Eds: M. I. Mishchenko, J. W. Hovenier, L. D. Travis), Academic, San Diego, CA **2000**.
[18] K. L. Kelly, E. Coronado, L. L. Zhao, G. C. Schatz, *J. Phys. Chem. B* **2003**, *107*, 668.
[19] a) L. R. Hirsch, R. J. Stafford, J. A. Bankson, S. R. Sershen, B. Rivera, R. E. Price, J. D. Hazle, N. J. Halas, *Proc. Natl. Acad. Sci. USA* **2003**, *100*, 13 549. b) C. Loo, A. Lin, L. Hirsch, M.-H. Lee, J. Barton, N. J. Halas, J. L. West, R. Drezek, *Technol. Cancer Res. Treat.* **2001**, *3*, 33.
[20] J. Huang, R. B. Kaner, *Nat. Mater.* **2004**, *3*, 783.
[21] a) Y. Yarden, M. X. Sliwkowski, *Nat. Rev. Mol. Cell Biol.* **2001**, *2*, 127. b) M. A. Molina, J. Codony-Servat, J. Albanell, F. Rojo, J. Arribas, J. Basela, *Cancer Res.* **2001**, *61*, 4744.

  